Extraction of negative ions from pulsed electronegative inductively coupled plasmas having a radio-frequency substrate bias

Pramod Subramonium[a)]
Department of Chemical and Biomolecular Engineering, University of Illinois, 1406 W. Green Street, Urbana, Illinois 61801

Mark J. Kushner[b)]
Department of Electrical and Computer Engineering, University of Illinois, 1406 W. Green Street, Urbana, Illinois 61801

(Received 5 August 2003; accepted 2 February 2004; published 27 April 2004)

Pulsed electronegative plasmas are promising candidates for reducing charge buildup during microelectronics fabrication by extracting negative ions into features. By modulating power in inductively coupled plasmas (ICPs), the plasma potential collapses during the power-off period, thereby allowing negative ions to be extracted. In principle, application of a radio-frequency (rf) substrate bias should accelerate these ions into features. In practice, this goal is not always achieved due to the unfavorable dynamics of the plasma potential. We computationally investigated the extraction of negative ions in the afterglow of pulsed ICPs having rf substrate biases sustained in Ar/Cl_2 gas mixtures. We found that the extraction of negative ions is optimized by delaying the transition to a capacitive heating mode in the afterglow, which can be achieved by the addition of Ar to Cl_2 plasmas. Increasing the bias voltage causes a capacitive heating mode to begin earlier, which prevents negative ions from being extracted. To circumvent this effect, schemes were investigated in which the rf bias is applied for only a portion of the pulse period. At high rf frequencies (≈ 10 MHz), ions striking the substrate have only thermal energies due to the majority of the applied bias being dropped across the bulk plasma. At lower frequencies (≈ 2 MHz), negative ions with 2–25 eV energy were extracted with an anisotropic angular distribution due to more favorable sheath formation. © *2004 American Vacuum Society.* [DOI: 10.1116/1.1690251]

I. INTRODUCTION

Pulsed electronegative plasmas are promising candidates for improving etch processes for microelectronics fabrication.[1–8] Extraction of negative ions from electronegative pulsed plasmas has been proposed as a method to reduce charge buildup in features, thereby reducing undesirable notching and bowing.[3] Negative ions are extracted from the plasma during the power-off phase and accelerated into the features neutralizing positive charge which typically accumulates at the bottom of features. The extraction of negative ions is generally possible during the power-off phase because the electron density and electron temperature drop to sufficiently small values that the charge balance in the plasma is sustained between negative and positive ions (an ion–ion plasma). Negative ions are able to escape the plasma when the plasma potential drops to values commensurate with the ion temperature as opposed to the electron temperature.

The pulsed systems of interest are typically inductively coupled plasmas (ICPs) powered at radio frequency (rf) where the carrier frequency (the power) is square wave modulated. An additional rf bias is capacitively applied to the substrate for ion acceleration. [The pulse repetition frequency (PRF) in these systems refers to the number of power-on and power-off modulation periods of the ICP power per second. The duty cycle refers to the fraction of a given modulation period that the power is on. The peak-power refers to the maximum instantaneous power applied during the power-on portion of the pulse.] Previous works on this class of pulsed plasmas were recently reviewed in Ref. 9. Additional works of interest to pulsed electronegative plasmas include the following.

Malyshev *et al.*[8] investigated pulsed ICPs in 10 mTorr Cl_2 at 300 W operated with a continuous rf substrate bias. They found that there was no significant difference in plasma characteristics with or without the rf bias during the ICP power-on period due to the high plasma density. However, during the ICP power-off period with a 12.5 MHz substrate bias, the electron temperature increased rapidly in the late afterglow after having decreased in the early afterglow. This behavior was attributed to a transition to a capacitive heating mode late in the afterglow. Sheath heating per electron increases with the increase in sheath speed and thickness accompanying the decrease in electron density.[10]

Kanakasabapathy *et al.*[11] observed that with low frequency (20 kHz) biases applied only in the afterglow of Cl_2 plasmas, one could obtain alternating fluxes of positive and negative ions to the substrate during the power-off period. Their conditions were Cl_2 at 1 mTorr with a peak ICP power of 300 W at 13.56 MHz, duty cycle 50% and PRF of 1 kHz. The peak bias voltage was 225 V.

Midha *et al.*[12] investigated the dynamics of ion–ion plas-

[a)]Present Address: Novellus Systems Inc., 11155 SW Leveton Dr., Tualatin, OR 97062; electronic mail pramod.subramonium@novellus.com
[b)]Author to whom correspondence should be addressed; electronic mail: mjk@uiuc.edu

mas with an rf bias using a one-dimensional fluid model. They observed that due to the lower temperature and larger mass of negative ions compared to electrons, the sheath structure in ion–ion plasmas differs significantly from that of conventional electron–ion plasmas. They investigated the consequences of rf bias frequency on the magnitude and energy of the ion flux incident on the electrodes. They found that operating at low bias frequencies (hundreds of kHz) is favorable for extracting high-energy ions from the plasma. They also observed the formation of double potential layers with positive and negative charges coexisting in the sheath at bias frequencies of tens of MHz.

Ramamurthi *et al.*[13] computationally investigated the dynamics of pulsed (square-wave modulated) chlorine ICPs (20 mTorr) without a substrate bias employing a two-dimensional continuum model. They found that the plasma separated into an electronegative core and an electropositive periphery during the activeglow and that an ion–ion plasma formed at about 15 μs into the afterglow. They observed a peak in electron temperature at power on and with a local maximum under the coil. They also observed that there were significant spatial dynamics of the negative ion density during the pulse, which were attributed to transport of negative ions toward the peak in the plasma potential during the activeglow and back diffusion to the boundaries during the afterglow.

In this article, a two-dimensional model is employed to investigate pulsed operation of Cl_2 and Ar/Cl_2 ICPs having rf substrate biases. A Monte Carlo simulation is additionally used to investigate the ion energy and angular distributions of positive and negative ions incident on the substrate during the afterglow period. We found that reducing the electronegativity of the plasma reduces the likelihood of sheath heating during the afterglow when using a continuous-wave (cw) bias, though it may not aid in the extraction of negative ions.[14] A pulsed bias scheme was investigated with the goal of reducing capacitive sheath heating during the afterglow with the result that negative ions could be extracted onto the substrate. At lower bias voltages, ≈ 50 V, using a pulsed rf bias method results in negative ion extraction for a longer period of time than using a cw bias. We found that at high rf bias frequencies (≈ 10 MHz), ions extracted onto the substrate have only thermal energies and broad angular distributions, while at lower bias frequencies ($\approx 1-2$ MHz), negative ions having energies of 2–25 eV are extracted with an anisotropic angular distribution.

Brief descriptions of the parallel hybrid model and ion Monte Carlo simulation used in this study are presented in Sec. II. The two-dimensional dynamics of pulsed Ar/Cl_2 plasmas having substrate biases are discussed in Sec. III. Our concluding remarks are in Sec. IV.

II. DESCRIPTION OF THE MODEL

The model employed in this investigation is a moderately parallel implementation of the hybrid plasma equipment model (HPEM). The parallel hybrid model (HPEM-P) is described in detail in Ref. 9 and so will be only briefly discussed here. Task parallelism is employed in HPEM-P to execute the electromagnetics module (EMM), electron energy transport module (EETM), and fluid kinetics module (FKM) of the HPEM in parallel as different tasks on three processors of a symmetric multiprocessor computer having shared memory. The model is implemented using the compiler directives provided in OPENMP[15] for shared memory parallel programming. In doing so, parameters from the different modules can be exchanged through shared memory on a frequent and, in some cases, arbitrarily specified basis without interrupting the time evolving calculation being performed in any other module. For example, the plasma conductivity and collision frequency are continuously updated during execution of the FKM. These updated parameters are made available in shared memory as they are computed so that they can be accessed by the EMM to produce nearly continuous updates of the electromagnetic fields. These more frequent updates of the electromagnetic fields are then made available to the electron Monte Carlo simulation (EMCS) of the EETM, through shared memory, along with parameters from the FKM to continuously update electron impact source functions and transport coefficients. The electron impact source functions and transport coefficients computed in the EETM are then transferred to the FKM through shared memory, as they are updated, to compute densities, fluxes, and electrostatic fields. Using this technique, the parameters required by different modules are made available "on the fly" from other modules. The methodology adequately captures long-term transients as it directly interfaces the short scale plasma time scales with the long-term neutral time scales.

The physics options used in this study are separate continuity, momentum and energy equations for the density, fluxes and temperatures of all heavy species (neutrals and ions), and Poisson's equation is solved for the electric potential. Drift–diffusion techniques are employed to obtain the electron density using a Scharffeter Gummel formulation for the electron fluxes.[16] Electron transport coefficients and excitation rates are obtained using the EMCS.[17] Many power-on and power-off cycles are computed to achieve a pulse-periodic steady state.

The energy and angular distributions of ions incident on the substrate were obtained using the Plasma Chemistry Monte Carlo Simulation (PCMCS). The PCMCS is discussed in detail in Ref. 18 and so will be only briefly described here. At the end of HPEM-P electron source functions, the phase and position dependent electric fields and advective flow fields are exported to PCMCS. The PCMCS launches pseudoparticles representing ions and neutral species during the rf cycle from locations weighted by the electron impact source functions obtained from HPEM-P. The trajectories of the pseudoparticles are followed in a time dependent fashion using interpolated electric fields (position and phase). Surface reactions are represented by reactive sticking coefficients. Particle-mesh algorithms are used to represent ion–ion, ion–radical, and radical–radical collisions. In doing so, statistics on the densities of radicals and ions are collected

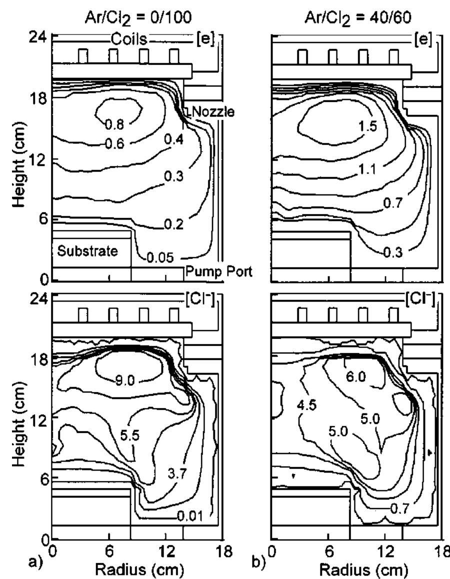

FIG. 1. Typical plasma properties at the end of the activeglow for pulsed operation of ICPs with cw substrate biases. (a) Cl_2 plasma properties: Electron density ($\times 10^{11}$ cm^{-3}) and Cl^- density ($\times 10^{10}$ cm^{-3}). (b) $Ar/Cl_2 = 40/60$ plasma properties: electron density ($\times 10^{11}$ cm^{-3}) and Cl^- density ($\times 10^{10}$ cm^{-3}). The conditions are a peak power of 450 W, PRF 10 kHz, gas flow rate 100 sccm, and pressure 10 mTorr. The cw substrate bias is 250 V at 10 MHz.

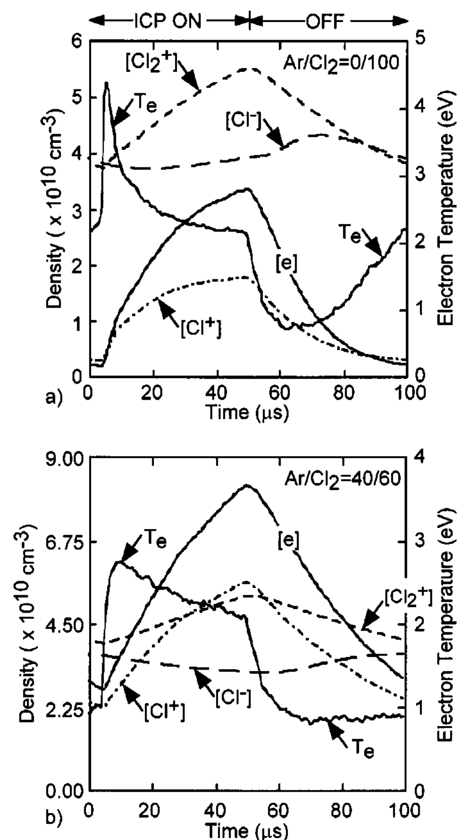

FIG. 2. Typical plasma properties for pulsed operation of ICPs with a cw substrate bias of 250 V at 10 MHz: (a) Cl_2 plasma properties and (b) $Ar/Cl_2 = 40/60$ plasma properties. Other conditions are ICP power 450 W, PRF 10 kHz, gas flow 100 sccm, and pressure 10 mTorr.

during the flight of the pseudoparticles and transferred to the mesh. The pseudoparticles then collide with the mesh defined densities. Statistics on the energy and angular distribution of selected charged and neutral species striking the substrate are collected. When all pseudoparticles either strike surfaces or are otherwise removed from the simulation by, for example, gas phase reactions, a computational iteration is complete. A converged solution is obtained by iterating through many flights (or launchings) of pseudoparticles.

III. PULSED Ar/Cl_2 PLASMAS WITH SUBSTRATE BIASES

Pulsed ICPs sustained in Cl_2 and Ar/Cl_2, with and without a cw substrate bias, were first investigated. The reaction mechanism for these mixtures is discussed in Ref. 9. The ICP reactor geometry was based on the experiments of Malyshev *et al.*[8] and is schematically shown in Fig. 1. The reactor height and radius are approximately 24 cm and 18 cm, respectively. The feedstock gases enter through nozzles located below the dielectric window. The reaction products are pumped out through a port surrounding the substrate. The ICP power is deposited from a four-turn coil placed on top of the dielectric window. The substrate diameter is about 16 cm. Validation of the model by comparison to experiments by Malyshev[8] is discussed in Ref. 10. The base case conditions are a pressure of 10 mTorr, time averaged ICP power of 225 W (peak power 450 W) at 10 MHz, cw substrate bias of 250 V at 10 MHz, PRF of 10 kHz, and duty cycle of 50%. The gas flow rate is 100 sccm. These conditions correspond to a 50 μs power-on pulse followed by a 50 μs afterglow. The base case plasma properties are shown in Fig. 1(a) where electron and Cl^- densities are shown at the end of the activeglow (power-on period) at 50 μs. The maximum electron density is 8×10^{10} cm^{-3}, peaked in the vicinity of the maximum power deposition beneath the coils, a distribution resulting from the collisional and attaching conditions. The peak plasma potential also occurs there, resulting in a maximum Cl^- density of 9×10^{10} cm^{-3}. The maximum electron temperatures are ≈ 3 eV.

Reactor averaged densities of Cl^+, Cl_2^+, Cl^-, and electrons, and the electron temperature are shown in Fig. 2(a) as a function of time for the base case. At the leading edge of the power-on pulse, the electron density is low, $\approx 3\times 10^9$ cm^{-3}, whereas the positive and negative ion densities are 4×10^{10} cm^{-3}, thereby constituting an ion–ion plasma. Upon application of ICP power, the electron temperature spikes, as a finite power is dissipated into a small inventory of electrons.[9] The resulting avalanche increases the Cl_2^+, Cl^+, and electron densities while not significantly increasing the Cl^- density. The rate coefficient for electron impact dissociative attachment to Cl_2 decreases with T_e, and so the rate of attachment decreases as T_e increases in the early activeglow. Electron heating by the substrate bias is negligible after about 10 μs of the power-on period due to the increase in electron density and decrease in sheath thickness, which reduces sheath heating. When the ICP power is terminated at

50 μs, the rapid decrease in T_e effectively shuts off further ionization while allowing the rate of attachment to increase. The electron and positive ion densities decrease while the negative ion density increases. In the absence of the rf substrate bias, T_e would continue to fall, eventually thermalizing with the gas temperature. Here, the electron temperature increases in the late afterglow.

In our earlier studies, we found that application of a cw rf substrate bias resulted in the transition to a capacitive heating mode late in the afterglow.[10] As the electron density decays in the afterglow, the sheath thickness λ_s above the substrate increases since $\lambda_s \sim n_e^{-1/2}$. As sheath heating scales with the square of the sheath speed, v_s, and $v_s \approx \omega\lambda_s$,[19] the total rate of sheath heating H, scales as $H \sim v_s^2 n_e$ which is then not a function of electron density. The specific heating rate (power per electron), h, scales as $H/n_e \sim 1/n_e$. Therefore, as the electron density decays, primarily by dissociative attachment to Cl_2, the sheath thickness λ_s increases which produces an increase in v_s and a net increase in specific heating rate h. A capacitive heating mode then begins. This results in an increase in (or slowing in the rate of decrease of) T_e. When h is sufficiently large (n_e sufficiently small) in the late afterglow that the electron sheath heating exceeds the rate of collisional loss, T_e increases. The capacitive heating slows the rate of decay in electron density as the increase in T_e provides for additional ionization sources and the increase in plasma potential provides for electron trapping.

For example, the electron density and temperature are shown in Fig. 3 for cw rf biases of 0, 75, 150, and 250 V for otherwise the base case conditions. In the absence of the bias, n_e and T_e monotonically decrease during the afterglow. Increasing the bias slows the rate of decay of the electron density and raises T_e in the afterglow at an earlier time due to the onset of sheath heating. Note that the spiking in T_e at the leading edge of the power-on pulse lessens with increasing bias due to the larger initial inventory of electrons. If the afterglow period is extended to a few hundreds of μs, the electron density eventually attains a quasisteady state corresponding to a capacitively coupled discharge. The substrate bias does not appreciably alter the plasma during the activeglow, as the electron temperature is nearly independent of bias, ≈2.5 eV. During the power-on pulse, the resulting large electron density shrinks the sheath and correspondingly reduces sheath heating from the bias.

The fluxes of electrons, and positive and negative ions to the substrate without and with a cw substrate bias are shown in Fig. 4. The positive ion flux is the sum of the fluxes of Ar^+, Cl^+, and Cl_2^+. Without the substrate bias, the fluxes of electrons and positive ions to the substrate are essentially equal during the power-on pulse, $\approx 2\times 10^{15}$ cm^{-2} s^{-1}. There are no negative ions extracted in the activeglow due to the large positive plasma potential. In the afterglow, the electrons decay due to dissociative attachment and diffusion to the walls. At about 25 μs into the power-off phase, the electron density has decreased to the point that charge neutrality is maintained by negative ions. That is, the electron density falls below the ambipolar limit and negative ion extraction

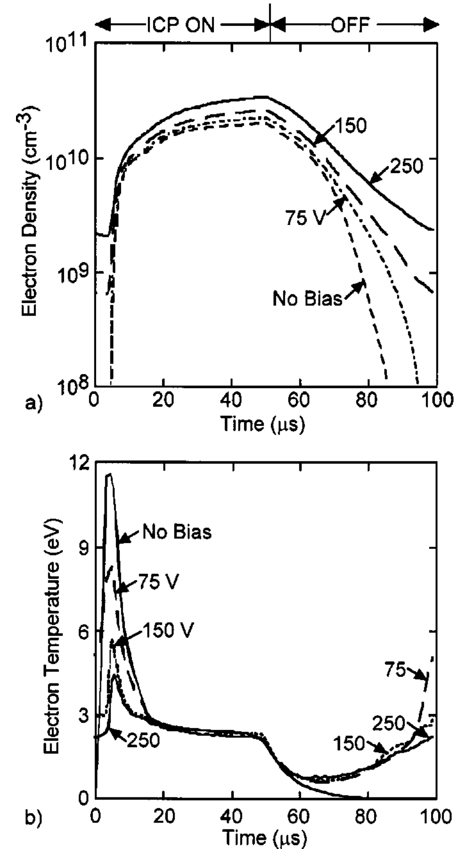

FIG. 3. Plasma properties in a Cl_2 ICP as a function of time for different rf bias voltages. (a) Reactor averaged electron density and (b) reactor averaged electron temperature. Operating conditions are peak ICP power 450 W, PRF 10 kHz, gas flow 100 sccm, and pressure 10 mTorr. Steady-state electron densities at the end of activeglow are similar for all bias voltages. The plasma transitions to being capacitively coupled at higher bias voltages with electron densities $\approx 10^9$ cm^{-3} in the afterglow.

begins. If the power-off period is long enough, the positive and ion fluxes will equilibrate with only a small fraction of the flux to the substrate being contributed by electrons.

With a cw substrate bias of 250 V, plasma quasineutrality is maintained by electrons and positive ions for the entire pulse period and no negative ions are extracted. The flux to the substrate consists exclusively of electrons and positive ions, as shown in Fig. 4(b). The small differences between electron and positive ion flux are due to the fluxes collected at other surfaces in the reactor. With or without a substrate bias, the activeglow is electron dominated with a large positive plasma potential and no negative ion extraction is obtained. With a cw substrate bias, sheath thickening in the afterglow and the maintenance of a large plasma potential prevents negative ion extraction. In extreme cases, the onset of capacitive coupling and an increase in electron temperature merely add to the potential barrier preventing extraction of negative ions. The oscillations in electron density in Fig. 4(b) will be discussed below.

One of the purposes of pulsed ICP sources with substrate biases is to accelerate negative ions into features. The onset of a capacitive heating mode, as indicated by the increase in T_e, in large part prevents this from happening due to the

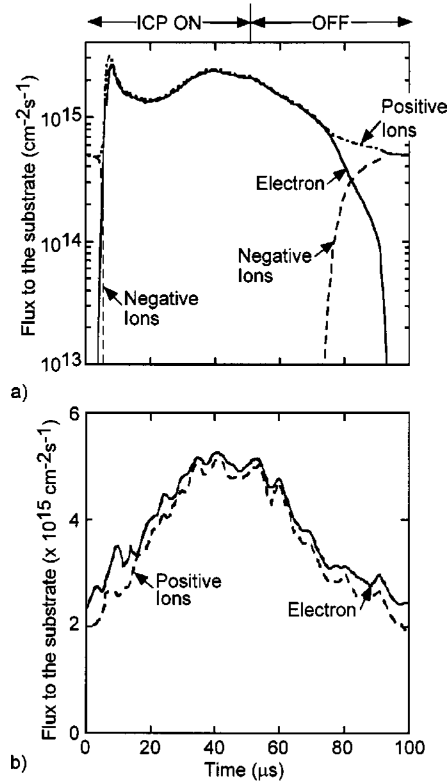

FIG. 4. Positive ion (Cl^+ and Cl_2^+), electron, and Cl^- fluxes to the substrate in Cl_2 ICPs with a peak ICP power of 450 W, PRF of 10 kHz, gas flow of 100 sccm, and pressure of 10 mTorr: (a) without a substrate bias and (b) with substrate bias of 250 V. With a bias, the sheath thickens during the afterglow, the plasma transitions to a capacitive heating mode, and there is no negative ion extraction.

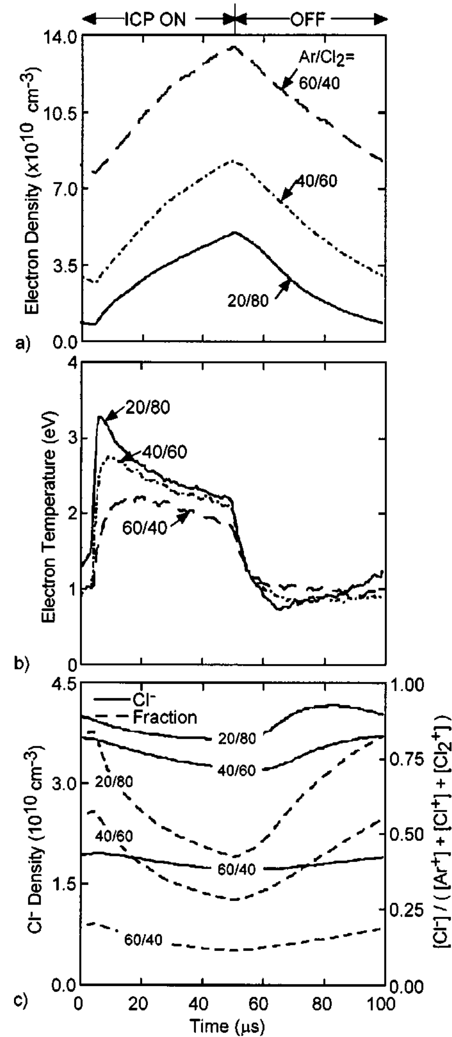

FIG. 5. Plasma properties in an Ar/Cl_2 ICP as a function of time for different Ar fractions (20%, 40% and 60%): (a) electron density, (b) electron temperature, (c) Cl^- density and ratio of negative ion density to positive ion density. Conditions are: Peak ICP power 450 W, rf bias 250 V, PRF 10 kHz, gas flow 100 sccm, and pressure 10 mTorr. Sheath heating decreases as the plasma becomes less electronegative with addition of Ar. The modulation in electron density due to dissociative attachment decreases at higher Ar percentages.

reestablishment of large positive plasma potentials. Earlier results[10] indicated that for a given set of operating conditions (e.g., power, pressure, gas mixture, PRF, and duty cycle), there is a critical bias voltage above which a capacitive heating mode will be established during the afterglow. Operating below this critical value is necessary in order to optimally extract negative ions.

Sheath heating can be decreased by maintaining the electron density above a critical value. This can be accomplished by decreasing the electronegativity of the Cl_2 plasmas by adding Ar. Toward this end, we investigated pulsed Ar/Cl_2 ICPs with a continuous substrate bias varying the Ar percentage from 0% to 60%. The base case conditions are 10 mTorr, time averaged ICP power of 225 W (peak power 450 W) at 10 MHz, continuous substrate bias of 250 V at 10 MHz, PRF of 10 kHz, and duty cycle of 50%. The base case plasma properties for an $Ar/Cl_2 = 40/60$ mixture with a cw rf bias are shown in Fig. 1(b) where electron and Cl^- densities are shown at the end of the activeglow (power-on period) at 50 μs. The maximum electron density is 1.5×10^{11} cm^{-3}, peaked in the vicinity of the maximum power deposition beneath the coils. The peak plasma potential also occurs there, resulting in a maximum Cl^- density of 6×10^{10} cm^{-3}.

Plasma properties for an $Ar/Cl_2 = 40/60$ mixture are shown in Fig. 2(b) as a function of time. The electron density and temperature, and Cl^- density for different Ar fractions are shown in Fig. 5. As the Ar percentage is increased, the modulation in electron density during the power-off phase decreases as the total rate of attachment to the smaller percentage of Cl_2 (which is also more highly dissociated) decreases. The electron density in the late afterglow increased from about 8×10^9 cm^{-3} to 8×10^{10} cm^{-3} as the Ar fraction increased from 20% to 60% as shown in Fig. 5(a). The transition from an electron–ion plasma to an ion–ion plasma is delayed at higher Ar fractions as the electron loss due to dissociative attachment is decreased, thereby delaying the thickening of the sheath. This delay is evident from the smaller ratio of negative ion density to positive ion density at larger Ar fractions.

To extract negative ions, the plasma should transition to an ion–ion plasma with quasineutrality maintained by posi-

tive and negative ions. Although this condition is favored at lower Ar percentages, it is not a sufficient condition for negative ion extraction as one must also avoid capacitive coupling and heating. Sheath thickening at lower Ar percentages eventually prevents extraction of negative ions by enabling this capacitive transition. For example, the higher electron temperatures in the late afterglow shown in Fig. 5(b) indicate sheath heating at lower Ar percentages. In pure Cl_2, the electron temperature in the late afterglow can be greater than the steady-state electron temperature in the late activeglow due to sheath heating.

The Cl^- density as a function of Ar fraction, shown in Fig. 5(c), also indicates that the plasma is progressively less electronegative as the Ar fraction increases. Not only is the Cl^- density smaller but there is also a smaller increase of Cl^- during the afterglow. If the goal is to extract negative ions in the afterglow, the plasma should transition to an ion–ion plasma with a minimum of sheath heating. In this regard, a gas mixture of $Ar/Cl_2 = 40/60$ is the best candidate as sheath heating is delayed until the end of the afterglow and there is a reasonably rapid transition to an ion–ion plasma.

The extraction of energetic negative ions with a substrate bias will always be difficult due to there being a fairly narrow window of operation. Large biases produce a capacitive heating mode early in the afterglow. Low electronegativities delay the onset of an ion–ion plasma. In this regard, we have investigated $Ar/Cl_2 = 40/60$ pulsed ICPs with both cw and pulsed rf substrate biases. The plasma conditions are a peak ICP power of 300 W at 10 MHz, rf bias of 100 V at 10 MHz, pressure of 10 mTorr, and flow rate of 100 sccm. Based on previous arguments, in this gas mixture, we might expect negative ion extraction as the plasma potential is low in the afterglow and the negative ion density is large. However, with a cw substrate bias of about 100 V, essentially no negative ions were extracted in the afterglow, as shown in Fig. 6(a). This result is attributed to the plasma transitioning to capacitive heating mode in the afterglow

To reduce the capacitive coupling, an alternate rf substrate bias sequence, shown in Fig. 6(b), was investigated. This is similar to the ion–ion synchronous biasing scheme employed by Kanakasabapathy *et al.*,[11] who defined such a scheme as a bias whose modulation envelope pulsed at an integral harmonic or subharmonic of the frequency of modulation of the ICP power. The ON and OFF periods of the substrate bias are phase locked to the ion–ion and electron–ion periods of pulsed operation, respectively, such that the bias is exclusively applied to the ion–ion plasma. In their studies, the ICP power (13.56 MHz) and the substrate bias (20 kHz) were pulsed at a PRF of 1 kHz and negative ion extraction was obtained. The low-frequency bias was applied during the afterglow after an initial delay of 15 μs resulting in alternating pulses of negative and positive ion fluxes to the substrate.

Our interest here is in the use of bias frequencies of many MHz, commensurate with the conventational ICP and capcitively coupled systems, and PRFs of the order of 10 kHz. With larger biases (>100 V), we observed that negative ion extraction is generally not obtained with a cw bias but can be

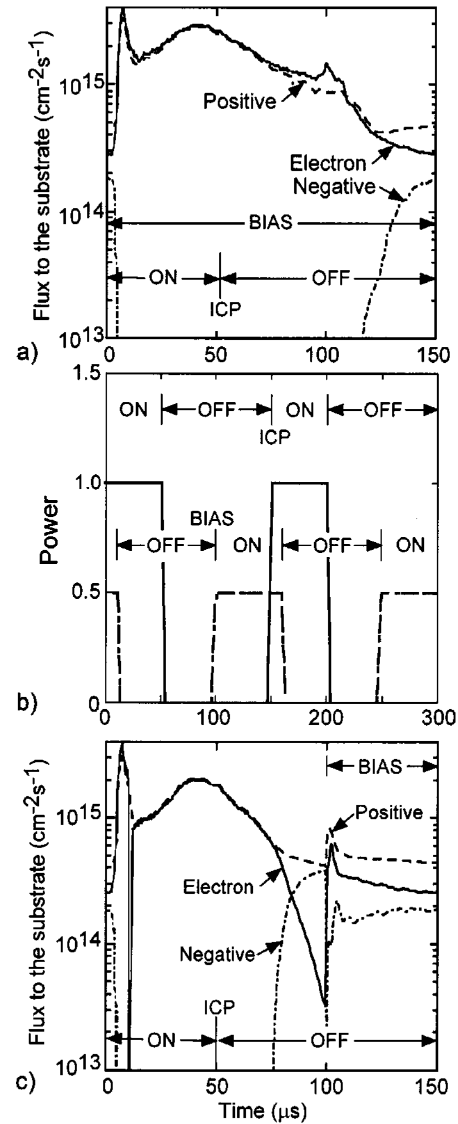

FIG. 6. Positive ion, negative ion, and electron fluxes to the substrate as a function of time for cw and pulsed bias schemes: (a) fluxes to the substrate with a cw substrate bias, (b) schematic of sequencing of pulsed ICP power and pulsed rf bias, and (c) fluxes to the substrate with a pulsed bias. Conditions are $Ar/Cl_2 = 40/60$ with a peak ICP power of 300 W, PRF of 6.67 kHz, duty cycle of 33%, gas flow of 100 sccm, and pressure of 10 mTorr. No negative ions are extracted with a cw rf bias as the plasma transitions to a capacitive heating mode. Negative ions are extracted with a pulsed rf bias as the transition to a capacitive heating mode is delayed.

obtained when the bias is applied only during the later portion of the afterglow. We attribute these trends to capacitive coupling being larger at higher biases and higher frequencies. Although an rf bias would normally be applied during the ICP power-on period for rapid etching, in this study, we apply the bias primarily during the afterglow. The bias scheme we demonstrate has the rf bias on during the last 50 μs of a 100 μs afterglow (PRF = 6.67 kHz, duty cycle 33%) and the first 10 μs of the power-on cycle. With this scheme for a bias amplitude of 100 V, significant negative ion extraction is obtained during the afterglow, as shown in Fig. 6(c). As there is no rf bias in the early afterglow, negative ions are extracted but, more importantly, the negative ions migrate

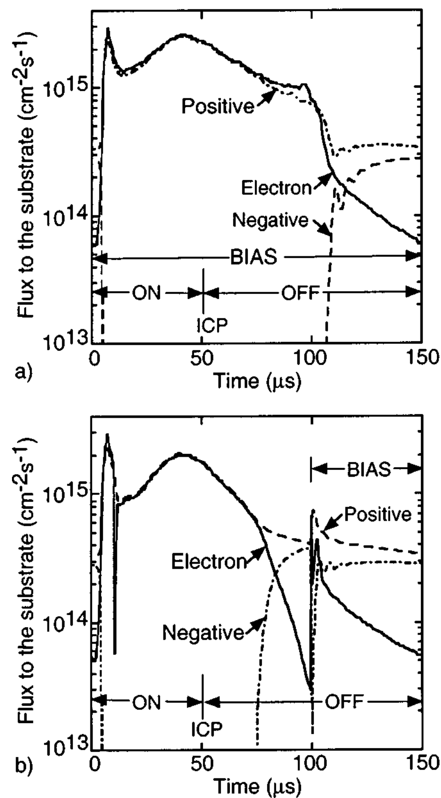

FIG. 7. Positive ion, electron, and Cl^- fluxes to the substrate in an $Ar/Cl_2 = 40/60$ ICP: (a) cw rf bias of 50 V and (b) pulsed rf bias of 50 V using the scheme shown in Fig. 6(a). (Operating conditions: Peak ICP power 300 W, PRF 6.67 kHz, duty cycle 33%, gas flow 100 sccm, and pressure 10 mTorr.) With a pulsed bias, negative ion extraction starts at about 75 μs and continues even after the application of the bias.

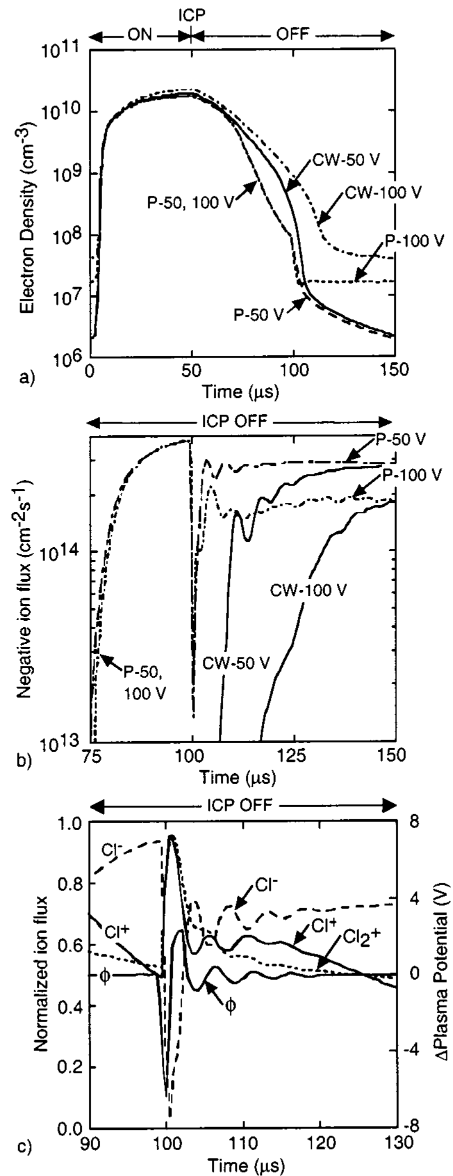

FIG. 8. Plasma parameters as a function of time for time for cw and pulsed rf biases: (a) electron density, (b) negative ion flux, and (c) normalized fluxes and plasma potential, ϕ. (Operating conditions: $Ar/Cl_2 = 40/60$, peak ICP power 300 W, PRF 6.67 kHz, duty cycle 33%, gas flow 100 sccm, and pressure 10 mTorr). "P-50 V" denotes a pulsed, 50 V bias. The negative ion flux in (b) is shown only for the last 75 μs of the afterglow. The ion fluxes in (c) are normalized. The plasma potential has been low-pass filtered to show the deviation from the rf cycle average value. With a cw bias of 100 V, the plasma transitions to capacitive heating mode with electron densities of about 4×10^7 cm^{-3}. With a pulsed bias, the plasma transitions from electron–ion to ion–ion plasma in the afterglow and negative ions are extracted from the plasma. The negative ion flux is larger with the pulsed bias.

from the core of the plasma to the sheath edge where they were previously excluded. When the bias is applied, the sheath thickens and electron flux is increased to sustain the current while the flux of negative ions decreases to $\approx 2\times10^{14}$ cm^{-2} s^{-1} from a prebias value of $\approx 4\times10^{14}$ cm^{-2} s^{-1}. Nevertheless, the negative ions still contribute about 10% of the negative flux to the substrate.

The division of the negative charged particle flux between electrons and ions is largely a function of the duty cycle of the bias and the rf voltage amplitude. For example, ion and electron fluxes are shown in Fig. 7 with a cw and pulsed bias of 50 V. With a 50 V cw bias, negative ions can be extracted in the afterglow starting at ≈ 110 μs both at an earlier time and with a larger flux than the 100 V cw bias. Using the pulsed scheme for a 50 V bias, negative ions are extracted prior to application of the bias, beginning at 70 μs, albeit with a low energy, and continue during the bias.

The magnitude of the applied bias voltage and the duration of the bias are keys to obtaining negative ion extraction in pulsed ICPs. These dependencies are summarized by the modulation of the electron density and negative ion fluxes shown in Fig. 8(a). With a cw bias of 50 V, the electron density monotonically decays during the afterglow, reaching 2×10^6 cm^{-3} at the end of the ICP power-off period, indicating a near absence of capacitive heating or electrostatic confinement. With a cw bias of 100 V, the electron density has a slower rate of decay in the afterglow, reaching only 4×10^7 cm^{-3} at the end of the ICP power-off period, a factor of 20 larger than with the 50 V bias. This indicates that the plasma is to some degree sustained by capacitive heating. With a pulsed bias of 100 V (beginning at 100 μs), the electron density decays more rapidly early in the afterglow in the absence of a bias, falling to about 2×10^7 cm^{-3}, but is then

clamped at this value when the bias starts, again indicating some degree of capacitive heating or electrostatic confinement. When using a pulsed 50 V bias, the decay of electron density is essentially the same as with the pulsed 100 V bias during the early afterglow, however the electron density continues to decay when the lower bias is applied, indicating a near absence of capacitive heating or electrostatic confinement. These conditions should be more conducive to negative ion extraction. Note that during the early afterglow, the electron density decays slower with the cw 50 V bias than with the pulsed biases, indicating some small degree of capacitive heating or electrostatic confinement.

The corresponding negative ion fluxes to the substrate are shown in Fig. 8(b) starting at 75 μs, 25 μs after the ICP power is terminated. In the absence of a bias (75–100 μs for the pulsed bias cases), as the plasma transitions to being ion–ion, the negative ion flux to the substrate increases, albeit with thermal energies, as discussed below. With application of the pulsed bias, there is an initial transient when the capacitive fields are established and the more mobile electrons provide current continuity. The negative ion fluxes eventually recover, more rapidly with the lower pulsed 50 V bias. With cw biases, negative ion fluxes slowly develop later in the afterglow than with the pulsed biases. The negative ion fluxes do eventually reach the same value late in the afterglow with either a cw or pulsed bias. With the cw biases, however, the fluence of negative ions is less since a longer period of time is required to initiate the flux, as discussed below.

Oscillations in predicted electron and ion fluxes [Figs. 4(b) and 8(b)] have been observed for select plasma conditions. The amplitudes of the oscillations are as large as 10%–20% but are typically smaller. Oscillations in electron densities, electron temperatures, and ion fluxes in electronegative inductively and capacitively coupled plasmas have recently been investigated by others in the context of ionization-attachment instabilities.[20,21] The frequencies of these instabilities vary with the feedstock gases, pressures, and power. For conditions comparable to ours, the frequencies are a few to tens of kHz which are commensurate with our PRF. The oscillations we observe are 150–200 kHz. These oscillations are likely not a result of attachment-ionization instabilities as the time constants for either attachment or ionization, which in large part determine the frequency of the instability, are longer than our oscillation periods. We also do not observe significant changes in plasma densities.

The oscillations we observe are likely initiated by the impulsive application of ICP power or bias voltage and are likely electrostatic wavelike in origin. For example, the ion fluxes to the substrate and plasma potential are shown in Fig. 8(c) for the pulsed 50 V bias case. The ion fluxes for Cl^-, Cl^+, and Cl_2^+ are normalized to approximately the same amplitude. The plasma potential in the presheath 1 cm above the substrate has been low-pass filtered to show only the deviation from its rf cycle averaged value. The oscillation of the plasma potential and positive ion fluxes are approximately in phase whereas the oscillation of the negative ion flux is 180° out of phase. The interpretation is that an electrostatic oscillation locally modulates the plasma potential, alternately increasing or decreasing the electric field which accelerates ions into the substrate. This enhances the flux of positive and negative ions on alternate half cycles. For this case, oscillations from previous impulses have damped out prior to the turn on of the rf bias and are reinitiated by the reestablishment of the sheath by the impulsive turn on of the bias. The frequencies of the oscillations are akin to ion acoustic waves. The amplitude of the oscillations in the flux of the heavier Cl_2^+ is smaller than those for Cl^+, and the damping periods are commensurate with ion collision frequencies, which would be consistent with this mechanism.

To alleviate charge buildup in the bottom of features, the negative ions should have an anisotropic angular distribution with energies which are significantly above thermal energies. Employing the PCMCS, we investigated the ion energy and angular distributions of the positive and negative ion fluxes to the substrate in the late afterglow. We observed that for rf biases of 50 V and 100 V at 10 MHz, although there is a significant flux of negative and positive ions to the substrate, the ions arrived with thermal energies having isotropic angular distributions.

These thermal distributions of ions are due in large part to the lack of a distinct sheath structure. At bias frequencies of tens of MHz, which are large compared to ion plasma frequency (≈ 1 MHz), and with the sheath thickening in the late afterglow, the rf period is much shorter than the ion transit time through the sheath. Ions experience time averaged electric fields over several rf cycles, and at these low pressures they should strike the substrate with an energy of about one-half of the rf amplitude. The complex sheath structure of ion–ion plasmas at these frequencies moderates incident ion energies.

For example, the plasma potential is shown in Fig. 9 for an $Ar/Cl_2 = 40/60$ ICP at 10 mTorr with a peak ICP power 300 W at 10 MHz, PRF of 6.67 kHz, duty cycle of 33.3%, and a pulsed rf bias of 100 V at 10 MHz. The plasma potential is shown at the end of the afterglow when the plasma is dominantly ion–ion for rf phases of 0, $\pi/2$, π, and $3\pi/2$. (Close-up views near the electrode are also shown for phases of 0 and π.) The electrode is most positive (100 V) at phase $\pi/2$ and most negative (-100 V) at phase $3\pi/2$. At these phases, the voltage is dropped over the bulk of the plasma rather than dominantly in the sheath with the electric field being monotonic across the plasma. The discharge has the appearance of a modulated dc glow discharge. The resulting electric fields are directed so that negative ions and positive ions are alternatively accelerated into the substrate but the fields are too weak to produce energetic ions. At $\phi = 0$ and $\phi = \pi$ the electric field is nonmonotonic. At these times, there is an inverted sheath near the electrode where the electrostatic fields reverses direction away from the electrode and should accelerate negative ions into the substrate. The duration and the magnitude of the field reversal are, however, insufficient to do so. Due to the lack of a significant sheath potential as the applied potential is largely dropped across

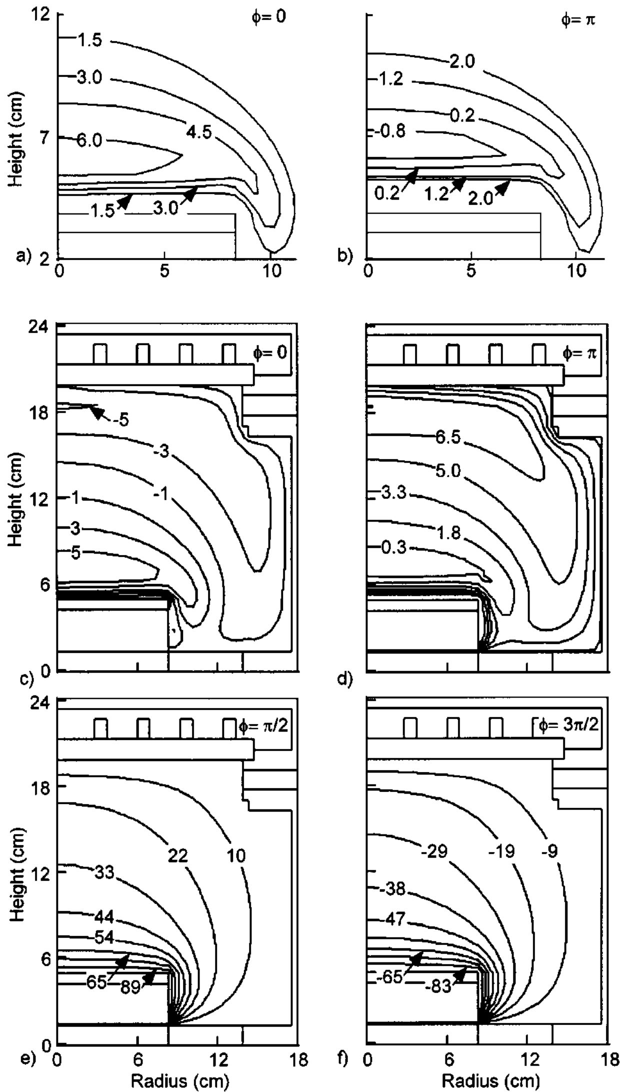

FIG. 9. Plasma potential at different phases ϕ during the rf period for an $Ar/Cl_2=40/60$ ICP: (a) $\phi=0$ (close-up), (b) $\phi=\pi$ (close-up), (c) $\phi=0$, (d) $\phi=\pi/2$, (e) $\phi=\pi$, and (f) $\phi=3\pi/2$. (Operating conditions: Peak ICP power 300 W at 10 MHz, PRF 6.67 kHz, duty cycle 33%, and pulsed rf bias of 100 V at 10 MHz.) The substrate voltage is largely dropped across the bulk of the plasma at 10 MHz. Weak inverted sheaths are formed near the substrate at $\phi=0$ and $\phi=\pi$.

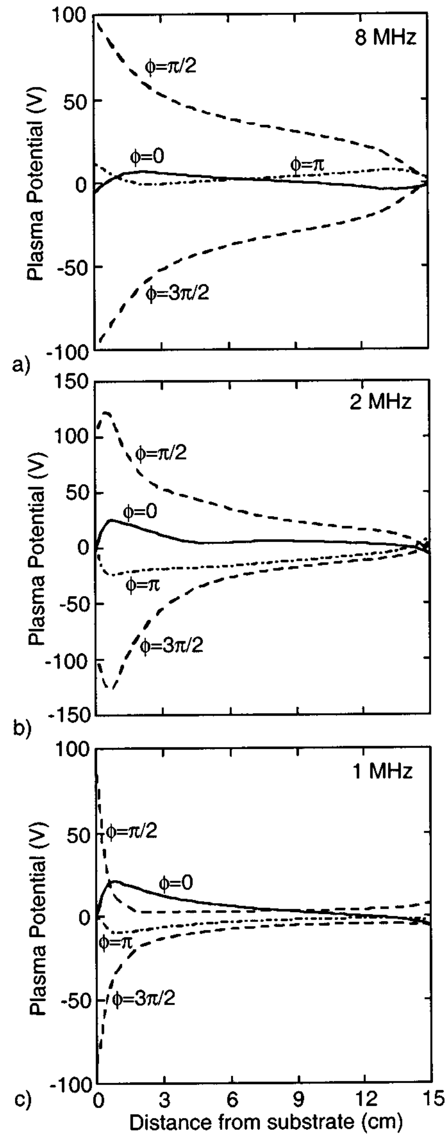

FIG. 10. Plasma potential as a function of height above the substrate at a radius of 1 cm for different phases in the rf period for an $Ar/Cl_2=40/60$ plasma: (a) bias frequency of 8 MHz, (b) 2 MHz, and (c) 1 MHz. (Operating conditions: Peak ICP power 300 W at 10 MHz, PRF 6.67 kHz, duty cycle 33%, and a pulsed rf bias 100 V.) At 8 MHz, the plasma has the appearance of a dc plasma with a large proportion of the applied bias dropped across the bulk of the plasma. At 1 MHz, most of the applied voltage is dropped close to the substrate.

the bulk plasma and due to a strong inverse field region near the electrodes, both positive and negative ions reach the substrate with only thermal energies and nearly isotropic angular distributions.

Midha *et al.*,[12] found that the frequency of the rf bias during the afterglow is important in determining the characteristics of the ion flux to the substrate. They concluded that operating at low bias frequencies (hundreds of kHz) is favorable for extracting high-energy ions from the plasma. Toward this end, we investigated pulsed substrate biases with frequencies of 1–10 MHz comparable to the ion plasma frequency (≈ 1 MHz) and commensurate with bias frequencies used in conventional reactors. For the lower frequencies, ions transit through the sheath in less than one rf cycle. The plasma potentials as a function of height at a radius of 1 cm for bias frequencies of 1, 2, and 8 MHz are shown in Fig. 10. At 8 MHz, the discharge still has the appearance of a modulated dc glow discharge with the applied bias largely dropped across the bulk of the plasma. The sheaths at $\phi=\pi/2$ and $\phi=3\pi/2$ should accelerate negative ions and positive ions (respectively) into the substrate but the electric fields are too weak. At 2 MHz, a sheath structure begins to form at $\phi=\pi/2$ and $\phi=3\pi/2$, although there is still a significant voltage drop across the bulk plasma indicative of the more resistive ion–ion plasma compared to an electron–ion plasma. The inverted sheath is present at all phases and which tend to slow negative ions at $\phi=\pi/2$ and positive ions at ϕ

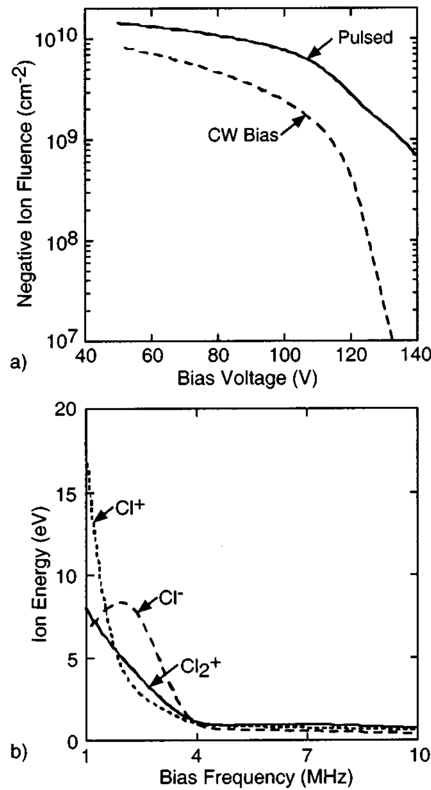

FIG. 11. Fluence of negative ions and average energy of ions incident on the substrate for an $Ar/Cl_2=40/60$ plasma: (a) negative ion fluence during the last 50 μs of the afterglow as a function of bias voltage and (b) average energy of Cl_2^+, Cl^+, and Cl^- incident on the substrate as function of bias frequency. (Operating conditions: Peak ICP power 300 W at 10 MHz, PRF 6.67 kHz, and duty cycle 33%.) Due to reduced capacitive heating with a pulsed bias, a larger fluence of negative ions is extracted. As the bias frequency decreases, the formation of sheaths increases the energy of negative ions incident on the substrate. Negative ions are extracted with an average energy of 9 eV at 2 MHz.

$=3\pi/2$. Since the fraction of the potential contained in the inverted sheath is small, the ions (both negative and positive) retain much of their inertia to the substrate. Alternatively, negative ions close to the electrodes are accelerated into the surface at $\phi=\pi$ and $3\pi/2$, as are the positive ions at $\phi=0$ and $\pi/2$. As the frequency is reduced to 1 MHz, the magnitude of the electric field in the sheath increases, with most of the bias voltage dropped within a distance of 1 cm. The inverted sheath is present only at $\phi=0$ and $\phi=\pi$ enabling unhindered acceleration of negative ions ($\phi=0$) and positive ions ($\phi=\pi$).

To quantify the effect of bias voltage and frequency on ion extraction, the fluence and average energy of ions striking the substrate were determined as a function of frequency. The conditions are an $Ar/Cl_2=40/60$ ICP at 10 mTorr with a peak power 300 W at 10 MHz, PRF of 6.67 kHz, duty cycle of 33%, and a pulsed rf bias varied from 50 V to 125 V for a bias frequency of 10 MHz. Fluences of Cl^- ions incident on the substrate during 50 μs in the afterglow (with bias) as a function of cw and pulsed rf bias voltage are shown in Fig. 11(a). At low voltage, the cw and pulsed biases yield comparable fluences, as capacitive coupling is not significantly different. However at higher voltages, the onset of capacitive coupling occurs earlier with cw biasing, increasing the plasma potential and thereby trapping more negative ions in the bulk of the plasma. The delay in capacitive coupling with the pulsed bias increases the total negative ion fluence.

The average energies of Cl_2^+, Cl^+, and Cl^- ions as a function of bias frequency as computed with PCMCS are shown in Fig. 11(b). The positive ion flux is composed of 0.6% Ar^+, 99% Cl_2^+, and 0.4% Cl^+. The negative charged particle flux is composed of 99.4% Cl^- and 0.6% electrons. The larger proportion of Cl_2^+ is a result of charge exchange from Ar^+ and Cl^+ with Cl_2 which, in the absence of ionization in the afterglow, converts the majority of the ions to Cl_2^+. Although negative and positive ions are extracted from the plasma at the end of the afterglow for a pulsed rf bias of 100 V at 10 MHz, they have thermal energies and an isotropic angular distribution due to the absence of a distinct sheath. As the frequency decreases, the sheath begins to thin, producing larger electric fields closer to the substrate. The average ion energy incident on the substrate thereby increases with decreasing frequency. The average energy of negative ions at first increases more rapidly with decreasing frequency before positive ions become more energetic. At 1 MHz, the average energy of Cl_2^+ ions and Cl^- ions is about 7 eV. These disparities result from subtle differences in the sheath structure. For example, the plasma potential at 1 MHz is not symmetric between the cathode and anodic phases. The lack of symmetry results from different mole fraction weighted mobilities of positive and negative charge carriers.

The ion energy distributions incident on and averaged over the substrate as obtained from the PCMCS are shown in Fig. 12 for an $Ar/Cl_2=40/60$ ICP with a peak ICP power of 300 W at 10 MHz, PRF of 6.67 MHz, duty cycle of 33%, and a pulsed rf bias of 100 V. Results are shown for 1 and 2 MHz. Negative ions having energies of 2–25 eV are extracted from the plasma. Negative ions are more energetic by a few eV at 2 MHz compared to 1 MHz whereas Cl^+ is more energetic at 1 MHz. The Cl^+ ion energy distribution broadens at the lower frequency as the plasma ion transit time becomes a smaller fraction of the bias period. In this regime, the ions begin to see the instantaneous bias voltage, a trend not seen with the heavier ion. The angular spreads of the ion distributions are less than 4°, sufficient to reach the bottom of moderate aspect ratio trenches.

IV. CONCLUDING REMARKS

A two-dimensional model has been employed to investigate pulsed operation of Cl_2 and Ar/Cl_2 ICPs with cw and pulsed rf substrate biases. In chlorine plasmas without a substrate bias, Cl^- ions are extracted with low energy after the sheath decays, and the plasma transitions from an electron–ion to an ion–ion plasma. With a cw substrate bias, the plasma transitions to a capacitive heating mode in the afterglow, which prevents negative ion extraction at all but small rf biases. Though reducing the electronegativity of the plasma reduces sheath heating, it may not necessarily aid in

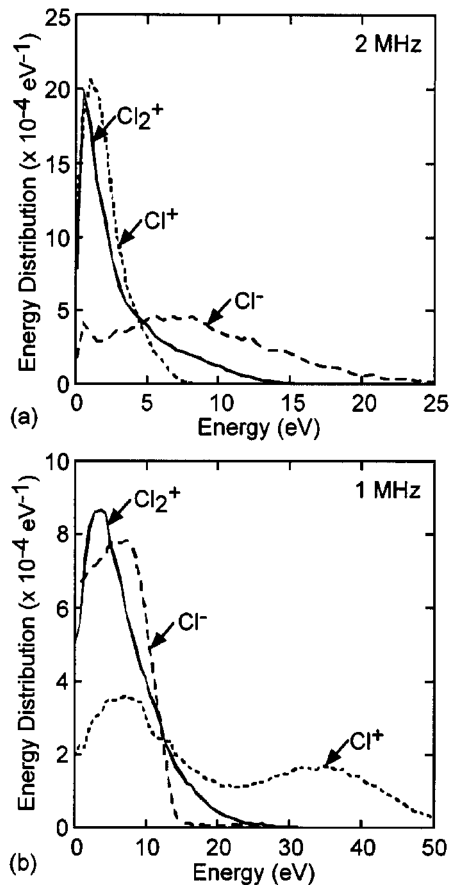

FIG. 12. Ion energy distributions onto the substrate at the end of the afterglow in an $Ar/Cl_2=40/60$ ICP with pulsed 100 V biases at (a) 2 MHz and (b) 1 MHz. (Operating conditions: Peak ICP power 300 W at 10 MHz, PRF 6.67 kHz, and duty cycle 33%). Negative ions are extracted with about 2–25 eV in the afterglow with a substrate bias of 2 MHz.

negative ion extraction. When using a pulsed rf bias in the afterglow, capacitive coupling is reduced and negative ion extraction is improved even at moderate biases of 100 V. The key to extraction of negative ions is to prolong the transition of the plasma to a capacitive mode. With a 10 MHz bias frequency, the ions extracted in the afterglow have only thermal energy as the applied rf voltage is largely dropped across the bulk plasma. At lower bias frequencies of 1–2 MHz negative ions with 2–25 eV energy are extracted with an anisotropic angular distribution.

ACKNOWLEDGMENTS

This work was supported by the National Science Foundation (CTS99-74962 and CTS03-15353), the Semiconductor Research Corporation, and Applied Materials Inc.

[1]L. J. Overzet, B. A. Smith, J. Kleber, and S. K. Kanakasabapathy, Jpn. J. Appl. Phys., Part 1 **36**, 2443 (1997).
[2]S. Samukawa and T. Meino, Plasma Sources Sci. Technol. **5**, 132 (1996).
[3]S. Samukawa and H. Ohtake, J. Vac. Sci. Technol. A **14**, 3049 (1996).
[4]S. Samukawa, Appl. Phys. Lett. **68**, 316 (1996).
[5]K. Takahashi, M. Hori, and T. Goto, Jpn. J. Appl. Phys., Part 2 **34**, L1088 (1993).
[6]T. Meino and S. Samukawa, Plasma Sources Sci. Technol. **6**, 398 (1997).
[7]M. V. Malyshev, V. M. Donnelly, S. Samukawa, and J. I. Colonell, J. Appl. Phys. **86**, 4813 (1999).
[8]M. V. Malyshev and V. M. Donnelly, Plasma Sources Sci. Technol. **9**, 353 (2000).
[9]P. Subramonium and M. J. Kushner, J. Vac. Sci. Technol. A **20**, 313 (2002).
[10]P. Subramonium and M. J. Kushner, Appl. Phys. Lett. **79**, 2145 (2001).
[11]S. K. Kanakasabapathy, L. J. Overzet, V. Midha, and D. Economou, Appl. Phys. Lett. **78**, 22 (2001).
[12]V. Midha and D. J. Economou, J. Appl. Phys. **90**, 1102 (2001).
[13]B. Ramamurthi and D. J. Economou, J. Vac. Sci. Technol. A **20**, 467 (2002).
[14]L. J. Overzet, B. A. Smith, J. L. Kleber, and S. K. Kanakasabapathy, Jpn. J. Appl. Phys., Part 1 **36**, 2443 (1997).
[15]Kuck and Associates, Inc. http://www.kai.com/parallel/kappro/
[16]Sharffeter-Gummel D. L. Scharfetter, and D. L. Gummel, IEEE Trans. Electron Devices **16**, 64 (1969).
[17]R. L. Kinder and M. J. Kushner, J. Vac. Sci. Technol. A **19**, 76 (2001).
[18]R. J. Hoekstra and M. J. Kushner, J. Appl. Phys. **79**, 2275 (1996).
[19]M. A. Lieberman and A. J. Lichtenberg, *Principles of Plasma Discharges and Materials Processing* (Wiley-Interscience, New York, 1994), Chap. 11.
[20]A. Descoeudres, L. Sansonnens, and C. Hollenstein, Plasma Sources Sci. Technol. **12**, 152 (2003).
[21]P. Chabert, A. J. Lichtenberg, M. A. Lieberman, and A. M. Marakhtanov, Plasma Sources Sci. Technol. **10**, 478 (2001).